

Creep and Hot Tensile Behavior of AISI 201LN Austenitic Stainless Steel



GUSTAVO HENRIQUE PELISSARI, DIOGO PEDRINO BRAGA,
 PEDRO HENRIQUE FERNANDES OLIVEIRA,
 DANIELLE CRISTINA CAMILO MAGALHÃES, MAURIZIO FERRANTE,
 CARLOS ALBERTO DELLA ROVERE, ANDREA MADEIRA KLIAUGA,
 LEVI DE OLIVEIRA BUENO, and VITOR LUIZ SORDI

AISI 200LN is a low nickel austenitic stainless steel (SS) in which nitrogen and manganese are used for nickel substitution. It shows excellent mechanical properties at room and cryogenic temperatures, with a lower production cost, if compared to the traditional 300 series SS. In spite of that, the performance of AISI 200 series SS under creep conditions remains largely underexplored in the literature. This study aims to assess the mechanical response of the AISI 201LN alloy when subjected to hot tensile and creep tests. The tensile tests were conducted at room temperature and in the range of 500 °C to 800 °C, whereas the creep tests were performed under constant load and within the temperature range 600 °C to 800 °C. Correlations among stress, temperature, secondary creep rate, rupture time, and creep ductility were obtained and results were compared to the literature data for the 300 series of traditional stainless steels. Based on the Zener–Hollomon parameter, constitutive equations were applied to describe the creep behavior of AISI 201LN within the range of stresses and temperatures used.

<https://doi.org/10.1007/s11661-021-06394-3>

© The Minerals, Metals & Materials Society and ASM International 2021

I. INTRODUCTION

AISI 200 series stainless steel (SS) production has been growing and changing remarkably with the partial replacement of nickel (Ni) by manganese (Mn) and nitrogen (N), thus allowing a considerable cost reduction.^[1,2] Although the 200 series steels had marginal applications in the 1980s and 1990s, more recently, improvements in melting practices have made it possible

to reduce the carbon and sulfur contents and add nitrogen, thus increasing the field of applications.^[3] The transformation-induced plasticity (TRIP) effect, which typically occurs in materials with low stacking fault energy (SFE), allows a considerable increase in strength and magnetic properties and promotes excellent energy absorption capacity. Furthermore, low SFE steels, as the AISI 200 series, are also prone to the phenomenon known as twinning-induced plasticity (TWIP), when the stress and strain rate conditions are favorable.^[4,5] Recently, this series of SS has been the focus of many studies addressing its mechanical behavior and the austenite reversion through thermo-mechanical treatments.^[6–8] Hamada *et al.*^[9] studied the effect of different tensile strain rates (5×10^{-4} and $1 \times 10^{-2} \text{ s}^{-1}$) at temperatures between -80 °C and 200 °C on two AISI 200 series stainless steels: 201 and 201L. The authors found that below room temperature, the TRIP effect was the dominant deformation mechanism, while TWIP and dislocation glide predominated in the range from 50 °C to 200 °C .

The chemical composition of SS AISI 201LN is similar to that of AISI 201, but with a lower C content ($C < 0.03 \text{ pct}$) and with the addition of N. In general, the deformation behavior of this family of SS is scarcely mentioned in the literature when compared to the traditional 300 series SS. At high temperatures, particularly under creep conditions, the performance of those

GUSTAVO HENRIQUE PELISSARI, DIOGO PEDRINO BRAGA, and PEDRO HENRIQUE FERNANDES OLIVEIRA are with the Graduate Program in Materials Science and Engineering, Federal University of São Carlos, Rodovia Washington Luiz, km 235 SP-310, São Carlos, São Paulo, 13565-905, Brazil and also with the Department of Materials Engineering, Federal University of São Carlos, Rodovia Washington Luiz, km 235 SP-310, São Carlos, São Paulo, 13565-905, Brazil. Contact e-mail: pelissari.gustavo.h@gmail.com DANIELLE CRISTINA CAMILO MAGALHÃES, CARLOS ALBERTO DELLA ROVERE, ANDREA MADEIRA KLIAUGA and VITOR LUIZ SORDI are with the Department of Materials Engineering, Federal University of São Carlos. MAURIZIO FERRANTE is with the Department of Mechanical Engineering, Federal University of São Carlos, Rodovia Washington Luiz, km 235 SP-310, São Carlos, São Paulo, 13565-905, Brazil. LEVI DE OLIVEIRA BUENO is with the STM - Sistemas de Teste em Materiais Ltda., Rua Argentina, 390-400, São Carlos, São Paulo, 13566-600, Brazil.

Manuscript submitted March 6, 2021; accepted July 8, 2021.

Article published online August 6, 2021

materials remains largely underexplored. This work aims to study the tensile behavior of an AISI 201LN SS at high temperatures by means of hot tensile tests, at temperatures between 500 °C and 800 °C, and by constant load creep tests in the temperature range of 600 °C to 800 °C. Results were compared to the literature data for the 300 series SS and constitutive equations were applied to describe the creep behavior of the AISI 201LN within a range of stresses and temperatures.

II. EXPERIMENTAL PROCEDURE

Samples of AISI 201LN austenitic SS were supplied by APERAM South America as plates having dimensions of 235 mm × 215 mm × 28 mm. The material was produced by continuous casting with a thickness of 200 mm, which is usually reduced to 5 mm or less by hot strip rolling. In the present case, the material was withdrawn from the middle of the rolling process to allow a more suitable volume of the samples. The chemical composition, as reported by the supplier, is in Table I.

The as received material (AR) was submitted to solution heat treatment (HT) at 1150 °C/30 min, under a vacuum environment, followed by cold water cooling. The microstructures of both conditions were observed by optical microscopy (OM). Electrolytic etching was performed using an aqueous solution with 10 wt pct of oxalic acid, at 12 V for approximately 30 seconds, at room temperature.

Tensile tests were performed at room temperature (RT) and 500 °C, 600 °C, 700 °C and 800 °C, according to ASTM E8 and ASTM E21 standards,^[10,11] employing a INSTRON 5500R machine, under an initial strain rate equal to $1 \times 10^{-3} \text{ s}^{-1}$. Three specimens were tested for each test condition. Constant load creep tests were carried out, according to ASTM E139,^[12] at temperatures in the range of 600 °C to 800 °C, in air, under nominal stresses going from 45 to 325 MPa. The creep tests were performed in creep machines, model STM-MF/1000; continuous recording of the specimen's elongation was measured by extensometers coupled to the test grips and connected to LVDTs, or potentiometric position sensors. For practical reasons, long-term creep tests were not replicated.

The specimens for creep and tensile tests were machined along the rolling direction of the as received plates; cylindrical specimens were thus obtained, as shown in Figure 1. All the tensile and creep tests were performed after solution heat treatments (HT condition).

III. RESULTS AND DISCUSSION

Figure 2 shows the microstructure of the material in the AR and HT conditions. The AR material shows essentially a recrystallized austenitic microstructure with an average grain size of $37 \pm 4 \mu\text{m}$ (measured by the linear intercept methods: ASTM E112^[13]), the presence

of twins (1), precipitates (2) and elongated δ -ferrite islands at the grain boundaries (3). The heat treatment was effective in dissolving the largest precipitates, increased the average grain size to approximately $61 \pm 4 \mu\text{m}$ and partially dissolved δ ferrite.

Figure 3 depicts representative engineering stress–strain curves obtained from tensile tests performed on the material in the HT condition, at RT, 500 °C, 600 °C, 700 °C, and 800 °C. The corresponding nominal tensile properties are in Table II, where $\sigma_{0.2}$, σ_u , ϵ_R , and RA are, respectively, the nominal values of 0.2 pct proof stress, ultimate tensile strength, strain at rupture, and reduction in area. In determining the strain hardening parameters (n' , K), the Hollomon's model ($\sigma = k\epsilon^{n'}$) was applied to the region of uniform plastic deformation (from $\sigma_{0.2}$ to σ_u) of the respective true stress–true strain curves.

From Figure 3(a) it is clear that at room temperature the material under study exhibits both strength and ductility higher than at high temperatures (except for ϵ_R at 800 °C, as commented further below). Even when compared to conventional AISI 304/316 stainless steels (in Figure 3(b)), 201LN showed a better combination of these properties at room temperature. This behavior is associated to the remarkable strain hardening capacity observed within the uniform plastic deformation regime. Previous studies^[8,9,14] have shown that SS 201LN is susceptible to martensitic transformation induced by deformation (the TRIP effect) which, in turn, enhances its capacity to absorb energy. Hence, the TRIP effect contributed to increase the deformation energy, a property quantified by the area under the stress-strain curve. In the present case, it was observed a change in the strain hardening exponent value (n' , from 0.3 to 0.8—see Table II) at approximately 30 pct of tensile strain, suggesting that deformation-induced martensite formation occurred during the tensile tests at room temperature. The presence of martensite in the necking region of the fractured specimens was confirmed by OM, in Figure 4(a).

As for the high-temperature tests, Figure 3 and Table II show that between 500 °C and 700 °C, the elongation at rupture (ϵ_R) and the reduction in area (RA) decrease to values around 50 pct. In the above temperature range, the presence of serrations in the curves, mainly at 600 °C, denotes a discontinuous plastic flow, indicating the occurrence of dynamic strain aging. It should also be noted that the uniform deformation capacity (represented by the values of ϵ_u and n' in Table II) decreases with increasing test temperature, contrary to the total elongation (ϵ_R). It means that as the temperature is increased, the observed increase in ϵ_R is due to non-uniform (after-necking) deformation. The insets in Figure 3(a) illustrate aspects of the necking region of the specimens, which appears narrowed at RT and extended at 800 °C. Particularly at 800 °C, the shape of the curve, with a large quantity of plastic deformation after σ_u , indicates that softening phenomena take place with increasing temperature. Flow softening is often related to dynamic recovery and dynamic recrystallization mechanisms which are associated, respectively, to

Table I. Chemical Composition (Wt Pct) of AISI 201LN Steel, as Reported by the Supplier

Cr	Mn	Ni	C	N	Mo	Si	Cu	S	P
17.02	6.87	4.02	0.027	0.16	0.02	0.40	0.02	0.001	0.03

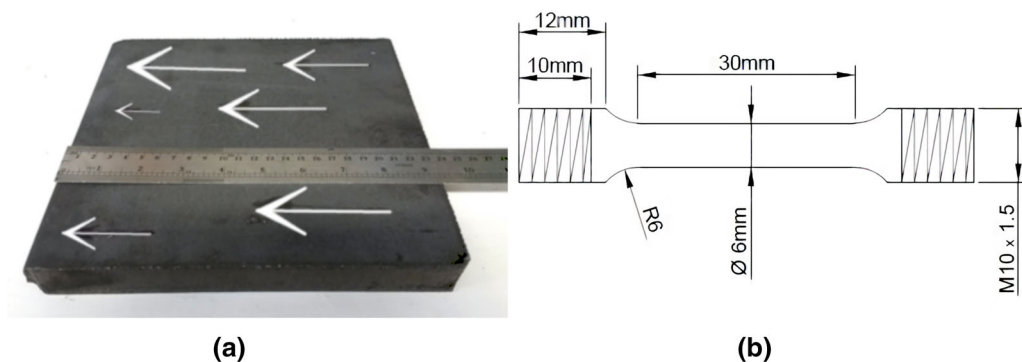


Fig. 1—As received material (a) and dimensional details of the specimens for creep and tensile tests (b). Arrows indicate the rolling direction.

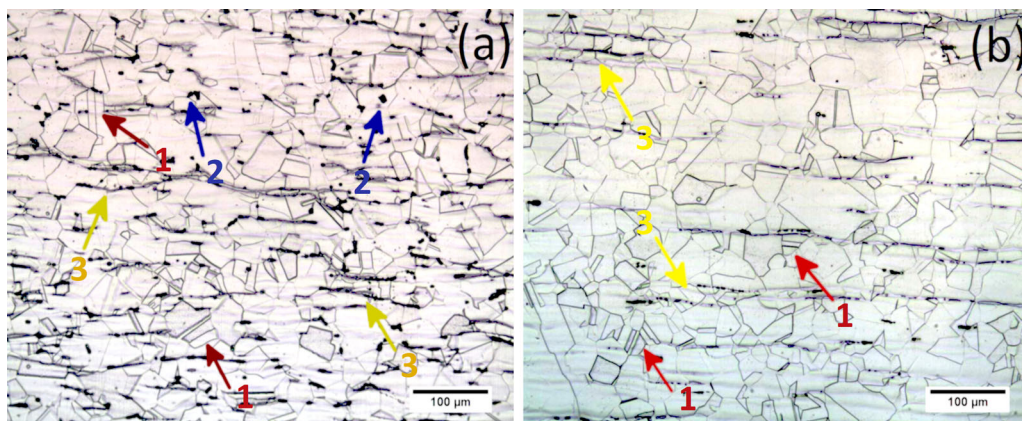


Fig. 2—Optical micrographs of AISI 201LN SS (longitudinal section), in the as received condition (a) and after solution heat treatment (b).

substructure coarsening and nucleation of new grains.^[16,17] Optical micrographs, taken in the necking region of the specimens (see Figure 4(b)), showed some evidence of small grains along boundaries of elongated grains in the austenitic matrix, reinforcing the suggestion that dynamic recrystallization occurred during the test. The numerous voids observed in Figure 4(b) also contributed to the increased non-uniform deformation at 800 °C. A more detailed microstructural analysis is not within the scope of the present work and further study is needed to elucidate the microstructural evolution of the material under different test conditions.

The comparison with typical literature data^[15] showed that the tensile properties of the AISI 201LN SS, under the present conditions, are comparable to those of the conventional austenitic SS AISI 304 and AISI 316 (see Figure 3(b)). AISI 201LN showed a tensile strength slightly higher than AISI 304 and lower than AISI 316, but similar ductility over the entire range of temperatures, except at RT, as already noted above. The better

properties of AISI 316 at the higher temperatures are due to its high Cr, Ni, and Mo contents, while the significantly higher strength and ductility of AISI 201LN at RT are due to the deformation-induced martensitic transformation during the test.

Figure 5 presents the creep curves obtained from constant load creep tests performed in air, at temperatures in the range of 600 °C to 800 °C, and stresses varying from 45 to 325 MPa (depending on the temperature level). The resulting rupture times (t_R) took place within the range of 1 to 3000 hours. In general, the total strain at rupture (ϵ_R) appears to increase with increasing test temperature. The steady-state creep rates ($\dot{\epsilon}_s$) were taken as the minimum values of the tangents ($\dot{\epsilon} = d\epsilon/dt$) on the creep curves shown in Figure 5.

The effects of stress and temperature on the rupture time are summarized in Figure 6, where a decrease in the creep strength is observed as the test temperature is increased. As expected, at higher temperatures, the work hardening capacity is reduced, while recovery and

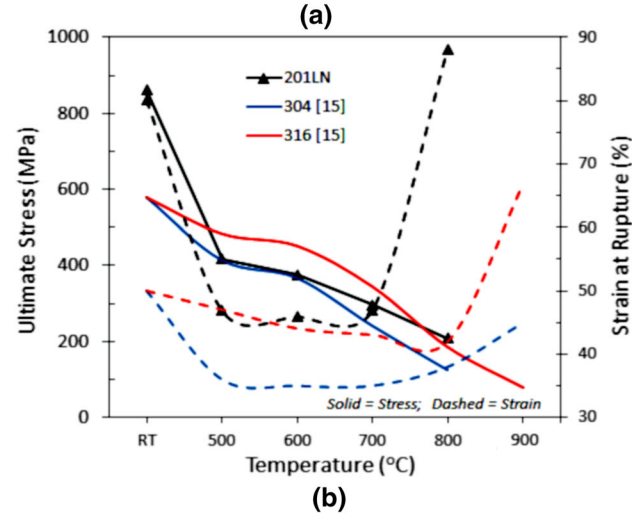
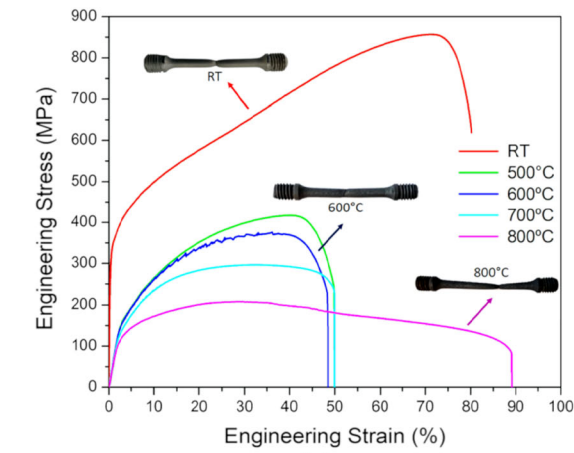


Fig. 3—Representative engineering tensile stress–strain curves at different temperatures for the solution-treated (HT) AISI 201LN (a). Comparison with typical literature data^[15] for AISI 304 and AISI 316 SS (b).

oxidation phenomena are favored, contributing to the loss in creep strength. In this figure, the present results are compared to a number of creep–rupture data of type 316LN SS collected by Kim *et al.*^[18] from worldwide literature surveys. These authors selected the creep data by the chemical composition defined for type 316 LN SS, especially a nitrogen content within the range of 0.06 to 0.15 wt pct. They compiled a total number of 345 data points, in the temperature range of 500 °C to 800 °C, which are represented by the dashed lines in Figure 6, for each temperature level. The comparison was made on typical results, without considering possible differences in grain size, processing route or other variables that may influence creep properties. Nevertheless, a good agreement among data was found, suggesting that the effect of temperature predominated over microstructural features, at least under a given range of testing conditions. With this proviso, it can be said that the AISI 201LN SS showed a creep resistance similar to type 316LN SS.

The steady-state creep rate ($\dot{\epsilon}_s$) has often been described as a function of stress and temperature by the expression in Eq. [1]^[19]:

$$\dot{\epsilon}_s = A\sigma^n \exp\left(\frac{-Q}{RT}\right), \quad [1]$$

where A is a constant, n is the power exponent of stress (σ), Q is an empirical activation energy for the creep rate controlling process, R is the universal gas constant and T is the absolute temperature. Equation [1] can be reduced to Eq. [2] for a set of creep tests performed at a given stress σ , or to Eq. [3] for tests performed at a given constant T .

$$\dot{\epsilon}_s = A'\exp\left(\frac{-Q}{RT}\right)\Big|_{\sigma}, \quad [2]$$

$$\dot{\epsilon}_s = B\sigma^n\Big|_T. \quad [3]$$

The apparent creep activation energy (Q), in Eq. [2], can be estimated through an Arrhenius-type diagram as shown in Figure 7, where $Q = -R[\delta(\ln\dot{\epsilon})/\delta(1/T)]_{\sigma}$ is the slope of the isostress lines. An average value of $Q = 525 \pm 34$ kJ/mol was obtained from the six straight lines shown in the figure. For pure metals and single-phase alloys, where dislocation climb is the rate controlling mechanism, values of Q close to the self-diffusion activation energy (Q_{SD}) are said to be expected.^[20,21] The values of Q determined here are higher than the self-diffusion of Fe, Cr or Mn in an austenitic matrix (~230 to 260 kJ/mol), but are in good agreement with the values determined from creep independent tests for types 304 and 316 SS (~410 to 560 kJ/mol).^[21,22] The higher values of Q obtained from specimens tested under the same stress at the different temperatures have been attributed to structural differences among the specimens (such as the presence of carbides and dislocation densities). However, if activation energy is determined after initially creeping specimens or by temperature change tests, the structure introduced at higher temperatures is assumed to remain constant, and values of Q closer to Q_{SD} can be obtained.^[21,22]

In Figure 8, the Norton's creep power law (Eq. [3]) was assumed to describe the dependence of the steady-state creep rate ($\dot{\epsilon}_s$) on stress, at distinct levels of temperature. Creep rates were plotted in a logarithmic scale, as a function of the normalized stress (σ/G), where G is the shear modulus at the corresponding temperature. Modulus compensation was applied as an attempt to more accurately describe the experimental data by a simple power law, since the dislocation substructure may be better related to the modulus-compensated stress rather than the applied stress.^[23]

From Figure 8, values of n ranging from ~6, at 800 °C (low stresses), to ~16, at 600 °C (high stresses), were obtained. As a general trend, the values of n increased with decreasing temperature and increasing stress. Moreover, at a given temperature, distinct breaks in the slope of the curves were observed, with higher n values at higher stresses. Although Eq. [1] suggests that n and Q are constant, most of the experimental results in the literature have shown that both parameters change with stress and temperature,^[24] as Figure 8 confirms.

Table II. Tensile Properties at Different Temperatures Obtained for Solution Heat-Treated (HT) AISI 201LN

T (°C)	$\sigma_{0.2}$ (MPa)	σ_u (MPa)	ϵ_R (pct)	RA (pct)	ϵ_u (pct)	n'	K (MPa)
25	321 ± 4	858 ± 7	80 ± 2	71 ± 2	72 ± 2	0.30/0.80 ± 0.01/0.03	1222/2456 ± 18/29
500	146 ± 4	417 ± 8	47 ± 1	54 ± 1	33 ± 1	0.42 ± 0.03	936 ± 15
600	133 ± 2	376 ± 5	46 ± 1	50 ± 1	31 ± 1	0.37 ± 0.02	804 ± 10
700	123 ± 2	297 ± 3	47 ± 1	49 ± 1	28 ± 1	0.31 ± 0.01	593 ± 8
800	98 ± 2	209 ± 3	88 ± 3	74 ± 2	26 ± 1	0.29 ± 0.01	401 ± 5

$\sigma_{0.2}$, yield strength; σ_u , ultimate tensile strength; ϵ_R , plastic strain at rupture; RA, reduction in area; ϵ_u , plastic strain at σ_u ; (n' , K) Hollomon's strain hardening parameters.

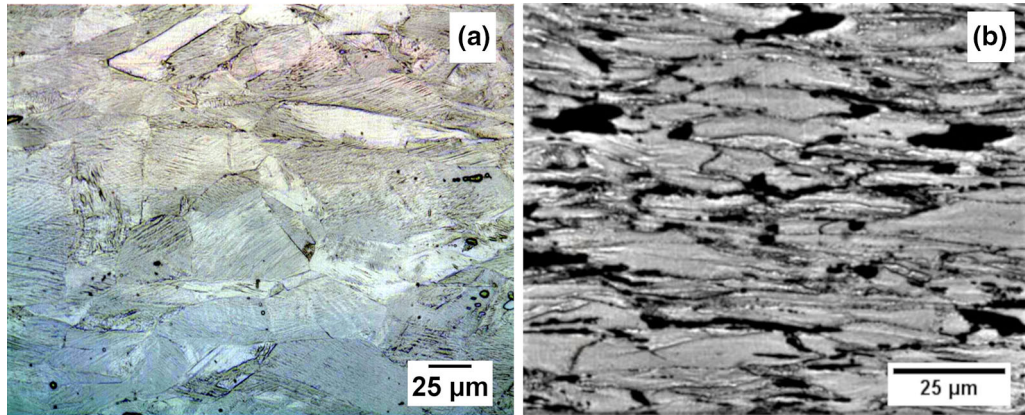


Fig. 4—Optical micrographs after tensile testing at RT (a) and 800 °C (b). Longitudinal section in the necking region of fractured specimens.

The combined effects of strain rate and temperature are often represented by the Zener–Hollomon^[25] parameter (Z), which represents a possibility of parameterizing Norton's diagram data according to a single reference curve, with a single apparent activation energy value (Q). Thus Eq. [1] can be rewritten as:

$$Z = \dot{\epsilon}_s \exp\left(\frac{Q}{RT}\right) = A\sigma^n. \quad [4]$$

A Zener–Hollomon diagram was constructed, see Figure 9, where the Z values are plotted on a logarithmic scale as a function of the normalized stresses (σ/G). A single average value of $Q = 525$ kJ/mol was chosen for the Z calculation. The slope of the parameterized curve is expected to be equivalent to the n -exponent of Norton's law (Eq. [3]) at the corresponding test conditions. In Figure 9 three distinct regions were selected as an attempt to quantify the variation of n with respect to the test conditions. As can be seen, this curve exhibits n values varying from ~ 5 (in the lowest stress range) to ~ 16 (in the highest stress range), which agree well with the range of n values presented in Figure 8.

Many authors have reported distinct breaks in this kind of curves. Values of n ranging from 1 (at low stresses) to 14 (at high stresses) have been commonly reported and associated to the predominance of different deformation mechanisms controlling the creep rate.^[24] In the first two regions of Figure 9, it can be suggested that the creep process was controlled by dislocation climb at high and medium temperatures, where n ranges

from ~ 5 to ~ 8 . At stress levels high enough to activate dislocation glide, high values of n can be expected. These here simplified hypotheses were discussed in detail by Langdon,^[26] in the context of pure metals and simple solid solution alloys. In the case of more complex alloys, the resulting creep rate may involve complex interactions due to the effects of precipitation, particle growth, phase transformation or damage accumulation, so that the proposed controlling mechanisms for simpler materials do not apply directly. Meanwhile, other authors have suggested that the value of n may vary continuously with stress and temperature, and that deformation occurs under the effect of an effective stress, given by the difference between the applied stress and an internal stress, or friction stress, which depends on the microstructural state and substructure deformation during creep.^[20,24]

Despite controversies regarding the nature of n and Q and the reason for their variations, Eq. [4], with discretely chosen values of n and Q remains useful in the assessment of materials' performance for practical purposes. In the present study, it was possible to identify three distinct regions in the curve in Figure 9, from which the parameters of the corresponding general creep equation were determined.

While the temperature sensitivity has been consistently represented by an Arrhenius-type equation, relationships other than Norton's power law (Eq. [4]) have been proposed to describe the stress dependence. Besides the Norton's relation (Eq. [4]), Dorn's relation (Eq. [5]) and Garofalo's relation (Eq. [6]) will be considered^[19]:

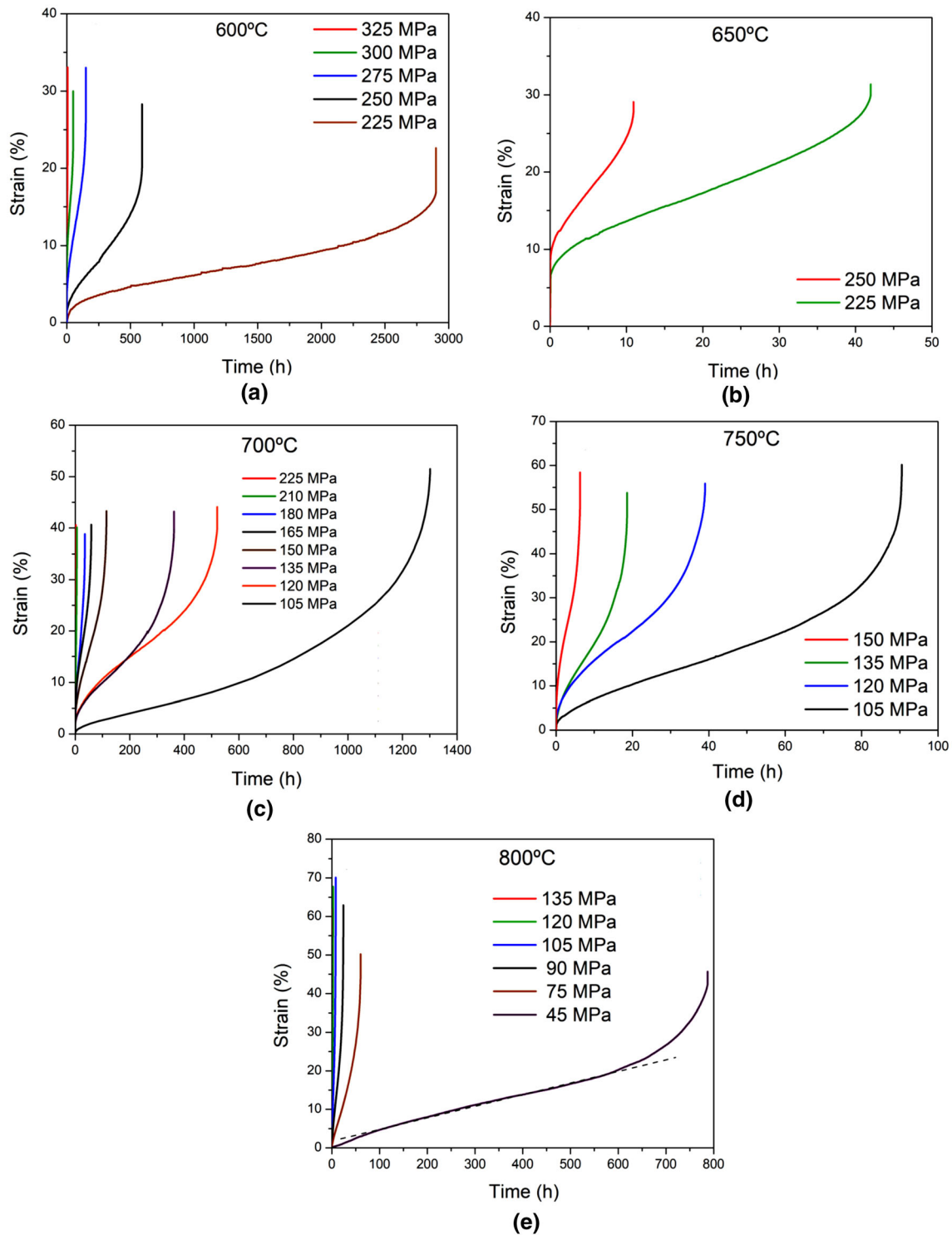


Fig. 5—Creep curves obtained at 600 °C (a), 650 °C (b), 700 °C (c), 750 °C (d), and 800 °C (e) for SS AISI 201LN. The dashed line in (e) represents the “steady-state creep rate” determined on the secondary stage of the curves.

$$Z = B' \exp(\beta\sigma), \quad [5]$$

$$Z = A'' [\sinh(\alpha\sigma)]^{n''}, \quad [6]$$

where Z is the temperature-compensated creep strain rate, B' , β , A'' , n'' and α are material constants.

The Dorn's relation is represented in linearized form in Figure 10, where $\ln(Z)$ is plotted as a function of the

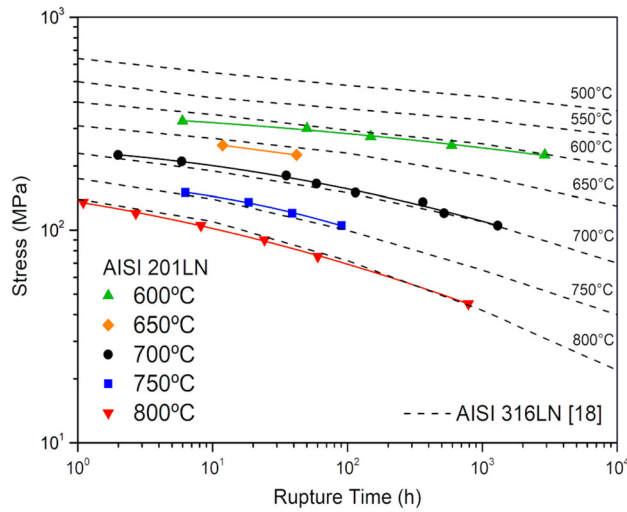


Fig. 6—Rupture times under constant load creep tests for AISI 201LN, compared with the representative literature data^[18] for AISI 316LN (dashed lines).

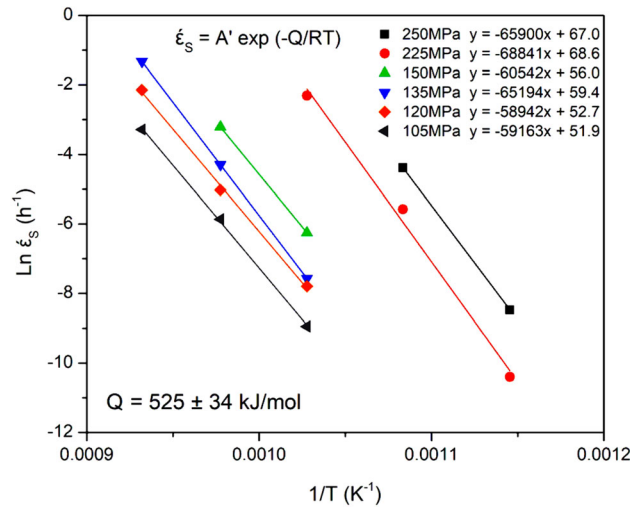


Fig. 7—Arrhenius plot and determination of apparent creep activation energy (Q) for AISI 201LN stainless steel.

modulus-compensated stress (σ/G), to determine the constants B' and β from Eq. [5]. As can be seen, an acceptable fit is obtained in Figure 10, suggesting that, under the present conditions, the dependence of the temperature-compensated creep rate on the modulus-compensated stress could be reasonably expressed in terms of a simple exponential relation.

In Figure 11, Garofalo's relation (Eq. [6]) was linearized in order to determine the values A'' and n'' . Again, the modulus-compensated stress (σ/G) was used (instead of σ) and a constant value of $Q = 525$ kJ/mol was considered. The constant α was roughly estimated as $\alpha \approx \beta/n$,^[27,28] with n and β taken from Figures 8 and 9, respectively. Although more accurate procedures have been discussed for the fit of the Garofalo equation,^[29,30] for the present purpose, Figure 11 represents an acceptable fit with the experimental data. According to Figures 10 and 11, Eqs. [5] and [6] can be considered as

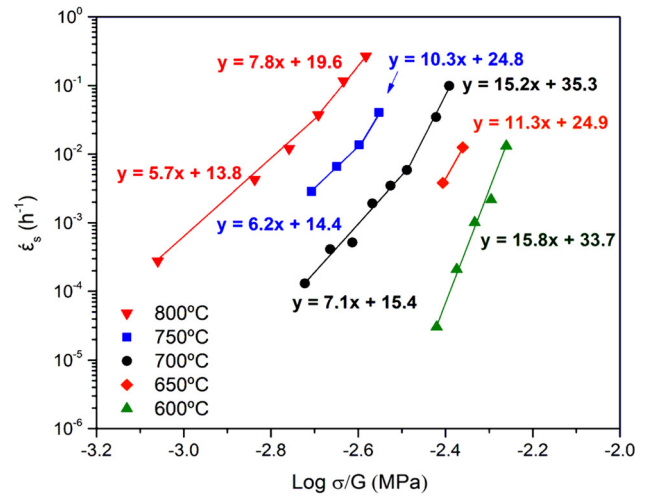


Fig. 8—Secondary creep rate ($\dot{\epsilon}_s$) as a function of the modulus-compensated stress (σ/G) and determination of the of the Norton's power law parameters.

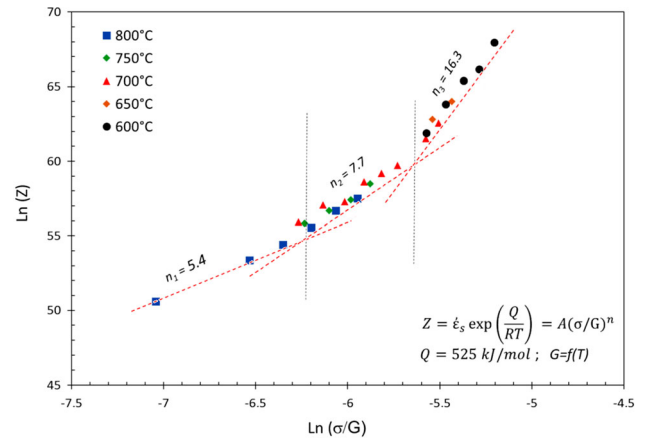


Fig. 9—Zener-Hollomon diagram for AISI 201LN stainless steel.

suitable constitutive equations to describe the dependence of creep rate on stress and temperature.

Table III summarizes the constitutive equations with their respective constants, as determined for the AISI 201LN SS under the present range of creep condition. Since the creep behavior of this class of SS remains largely unexplored in the literature, Table III offers a useful comparative basis for practical purposes.

The Monkman-Grant (M-G) model^[31] relates the steady-state creep rate ($\dot{\epsilon}_s$) and the rupture time (t_R). The M-G relationship (Eq. [7]) has been shown to be valid for many metals and alloys under a wide range of creep conditions, with the m -exponent generally reported to be close to 1.^[23]

$$\dot{\epsilon}_s \cdot t_R^m = K. \quad [7]$$

The validity of the M-G model establishes a direct relationship between the steady-state creep rate and the total time to rupture, regardless of the different combinations of stress and temperature from which a given rate may have resulted. As a whole, the present set of

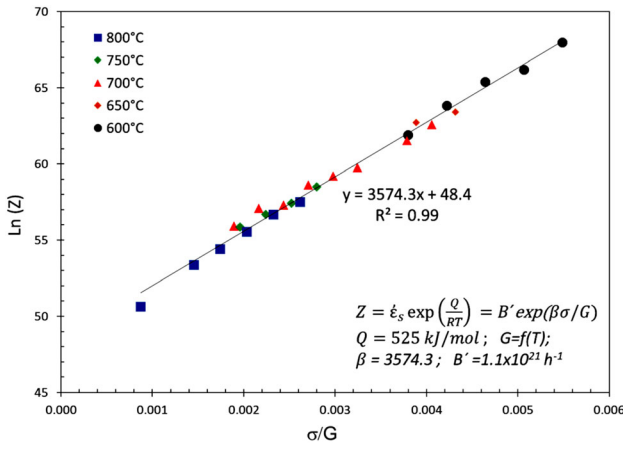


Fig. 10—Determination of the Dorn's equation parameters for constant load creep tests in AISI 201LN.

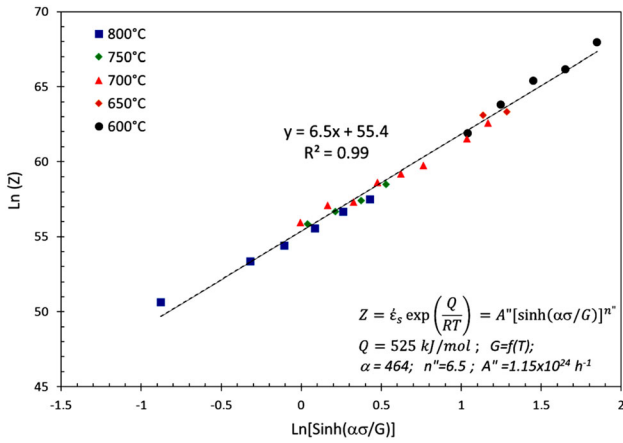


Fig. 11—Determination of the Garofalo's equation parameters for constant load creep tests in AISI 201LN.

data fits well with the M–G model, showing average values of $m = 1.07$ and $K = 0.26$, as shown in Figure 12. For a more detailed observation, the inset in this figure shows the values of m and K considering the distinct levels of temperature. While the value of m remains close to 1 (as expected), K tends to be slightly reduced with reducing temperature. It has been pointed out that a drop in the K value can be associated to precipitation effects occurring at the grain boundaries which hinder their mobility leading to a drop in the ductility of the material.^[32,33] In agreement with that, the tests performed at 600 °C and 650 °C, which showed the lower values of K in Figure 12, also exhibited some loss in ductility if compared to the tests at higher temperatures.

Equation [8] presents a modified Monkman–Grant (MMG) relation,^[34] where $m = 1$ and the rupture time t_R is divided by the total strain at the rupture ϵ_R .

$$\dot{\epsilon}_s \frac{t_R}{\epsilon_R} = C_{MMG}. \quad [8]$$

The constant $C_{MMG} = 0.47$ shown in Figure 13(a) is close to that mentioned by Sundararajan^[35] for an AISI 304 SS. The author also shows values of C_{MMG} for different materials, ranging from 0.1, for a 2.25Cr–1Mo alloy, to 0.8 for a Ni–8Al alloy. The value of C_{MMG} can be interpreted as a measure of the contribution of the secondary stage to the total deformation obtained in the test, so that low values of this constant suggest that a large part of the creep strain is derived from tertiary creep.^[36] Conversely, when C_{MMG} approaches unity, it means that the tertiary stage is short and creep deformation occurs essentially in the steady flow regime.

The tertiary creep is related to the growth of damage, which increases the creep rate eventually resulting in failure. Based on a concept of continuous accumulation of creep damage, the creep damage tolerance factor λ is defined as the relationship between the total deformation at rupture ϵ_R and the deformation of the secondary stage, *i.e.*, the product $(\dot{\epsilon}_s \cdot t_R)$. It is considered an indicator of the susceptibility of a material to localized cracking and also an indicator of creep ductility.^[37]

$$\lambda = \frac{\epsilon_R}{\dot{\epsilon}_s t_R}. \quad [9]$$

It should be noted that $\lambda = 1/C_{MMG}$, and ϵ_R/t_R in Eq. [9] represents the average creep rate throughout the test. From Eq. [9], λ can be determined as the intercept at $\dot{\epsilon}_s = 1$ on a double logarithmic plot of (ϵ_R/t_R) vs. $\dot{\epsilon}_s$, as shown in Figure 13(b).

The value of $\lambda = 2.1$ obtained for AISI 201LN coincides with that determined by Phaniraj *et al.*^[37] for an AISI 304 steel. Figure 13(b) also includes dashed lines representing the behavior of a 9Cr–1Mo steel, which showed values of λ equals to 5 and 10, when tested in high and low stress regimes, respectively. High values of λ mean a significant contribution of tertiary stage in defining total strain and rupture time. Thus, several authors seek to associate it with the creep deformation mechanism: when $\lambda = 1$, it is assumed that most of deformation takes place in the secondary stage and low ductility and brittle fracture are expected; when $\lambda = 1.5$ to 2.5 it has been suggested that damage accumulation is due to cavity growth resulting from diffusional creep and dislocation climb (power law). Higher values of λ indicate resistance to local cracking, with ductile fracture and a significant necking effect.^[38,39] Figure 13 illustrates the constancy of λ and C_{MMG} for AISI 201LN throughout the investigated range of stress and temperature.

A number of techniques for creep rupture parameterization have been suggested in the literature^[24,40,41] aiming to extrapolate the mechanical responses obtained in short/medium duration tests to real service conditions. On this respect, Figure 12 shows the results of the Larson–Miller methodology, where the applied stress was plotted as a function of the Larson–Miller parameter (LMP), defined as:

$$LMP = T(C + \log t_R). \quad [10]$$

Table III. Constitutive Equations for Steady-State Creep Rate ($\dot{\epsilon}_s$) for AISI 201LN for a Range of Creep Testing Conditions

	$\ln Z$	σ (MPa)	T (K)	Creep Strain Rate (h^{-1})*
Norton (Eq. [4])	50 to 55	45 to 90	1073	$\dot{\epsilon}_s = 3.66 \times 10^{38} (\frac{\sigma}{G})^{5.4} \exp(\frac{-525 \times 10^3}{RT})$
	55 to 60	90 to 210	973 to 1073	$\dot{\epsilon}_s = 9.59 \times 10^{44} (\frac{\sigma}{G})^{7.7} \exp(\frac{-525 \times 10^3}{RT})$
	60 to 68	210 to 325	873 to 973	$\dot{\epsilon}_s = 2.0 \times 10^{66} (\frac{\sigma}{G})^{16.3} \exp(\frac{-525 \times 10^3}{RT})$
Garofalo (Eq. [6])	50 to 68	45 to 325	873 to 1073	$\dot{\epsilon}_s = 1.15 \times 10^{24} [\sinh(464(\frac{\sigma}{G}))]^{6.5} \exp(\frac{-525 \times 10^3}{RT})$
Dorn (Eq. [5])	50 to 68	45 to 325	873 to 1073	$\dot{\epsilon}_s = 1.1 \times 10^{21} \exp(3574 \frac{\sigma}{G}) \exp(\frac{-525 \times 10^3}{RT})$

* $Q = 525 \text{ kJ/mol}$ (Fig. 6); $R = 8.314 \text{ J mol}^{-1} \cdot \text{K}^{-1}$; $G = f(T)$ MPa.

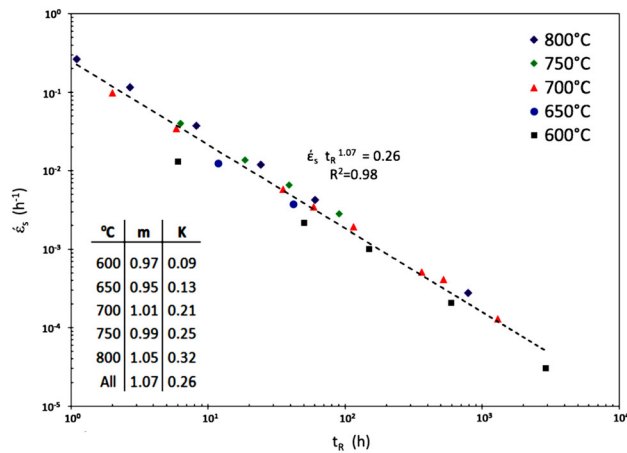


Fig. 12—Determination of Monkman–Grant parameters for AISI 201LN.

The constant C was estimated equal to 22.5 considering the pattern of isostress lines which were plotted on coordinate axes $\log t_R$ vs. $1/T$.^[41] Kim *et al.*^[18] reached a C value equal to 23 from a large number of literature creep data for type 316LN SS (N content between 0.06 and 0.15 pct), tested between and 500 °C and 800 °C. In order to compare these results, the same value of $C = 23$ is adopted in Figure 14. It can be seen that the two materials exhibit a very similar behavior, with 316LN slightly superior at higher stresses.

It has been reported that in several grades of steels the addition of nitrogen decreases SFE; Cr, Si, and Mn have the same effect, while Ni and C increase SFE.^[42] The AISI 201LN SS has a low SFE ($\sim 6.5 \text{ mJ/m}^2$),^[5] which provides resistance to creep, because recombination of partial dislocations required for cross-slipping is difficult. The addition of alloying elements, forming a solid solution, is the most effective way to increase creep resistance as some of them can decrease SFE to large extent.^[43] Mathew *et al.*^[44] reported that creep rupture strength was substantially increased with increase in N content of a 316L SS, which was attributed to solid solution strengthening, increase in Young’s modulus, decrease in SFE and carbonitrides precipitation.

Therefore, unlike the former austenitic SS stabilized with Mn (where a loss of resistance at high temperatures was associated with microstructural instability^[45]), the

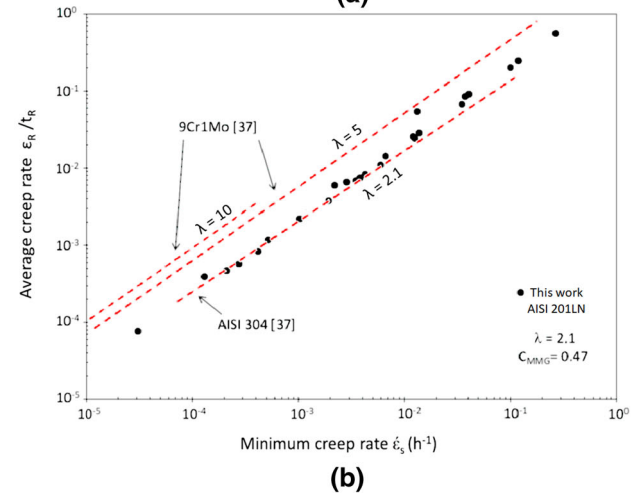
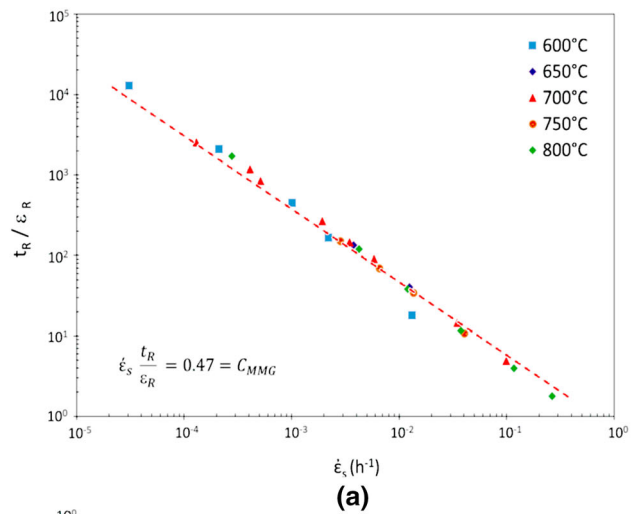


Fig. 13—Constancy of C_{MMG} (a) and λ (b) for AISI 201LN, compared to the literature data^[37] for different materials.

relatively high content of N of the AISI 201LN SS contributed to reduce SFE and to maintain resistance under prolonged exposure times, thus resulting creep properties comparable to those of some traditional austenitic SS, at relatively high temperatures. In this context, further work on the microstructural evolution under creep conditions is needed to allow safe service life predictions for this class of material.

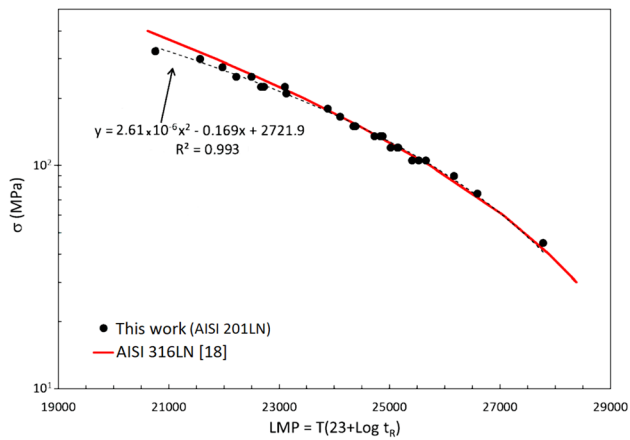


Fig. 14—Parameterization according to the Larson–Miller methodology for the AISI 201LN stainless steel, compared with the literature data^[18] for AISI 316LN.

IV. CONCLUSIONS

The tensile properties of the AISI 201LN SS, at temperatures between 500 °C and 800 °C, were found to be comparable to those of conventional austenitic SS. In this range of temperature, the AISI 201LN showed tensile strength slightly higher than AISI 304 and lower than AISI 316, with similar ductility. At room temperature, AISI 201LN showed a very high hardening capacity, which was attributed to the TRIP effect.

An approximately constant value for the apparent creep activation energy, $Q = 525 \pm 34$ kJ/mol, was estimated through an Arrhenius-type correlation between the test temperature and the secondary creep rate, from constant load creep tests performed at temperatures ranging from 600 °C to 800 °C and different levels of stress.

Constitutive equations, taken from the literature, were applied to describe the dependence of secondary creep rate on stress and temperature under the constant load creep tests. The Garofalo's model showed the best fit with experimental data and was considered as a suitable constitutive equation to describe the creep behavior of AISI 201LN SS under the present test conditions. As for the rupture time, the validity of the modified M–G relation and the constancy of the creep damage tolerance factor λ were verified here.

The Larson–Miller parameterization method was applied with a constant $C = 23$. The relation between the parameter LMP and the applied stress fitted well to form a master curve for AISI 201LN.

The comparison of the present results with literature data indicated that AISI 201LN shows creep properties similar to some traditional AISI 300 series austenitic SS at relatively high temperatures.

ACKNOWLEDGMENTS

Gustavo H. Pelissari acknowledges CAPES—Coordenação de Aperfeiçoamento de Pessoal de Nível Superior for his scholarship, Grant Number 88882.332698/2019-01. This study was financed in part by the Coordenação de Aperfeiçoamento de Pessoal de Nível Superior-Brasil (CAPES)-Finance Code 001, the Graduate Program in Materials Science and Engineering of the Federal University of São Carlos and the São Paulo Research Foundation (FAPESP)-Grant Number 2019/07178-6. The authors would like to thank the STM Materials Testing Systems, for the technical support in the creep tests, and the Aperam South America, for supplying samples of the 201LN material.

REFERENCES

1. J. Charles: *Rev. Metall.*, 2007, vol. 104, pp. 308–17.
2. ISSF: *Stainless Steel in Figures 2020*, ISSF-International Stainless Steel Forum, 2020. <https://www.worldstainless.org/statistics/stainless-steel-in-figures/>. Accessed 20 Jan 2021.
3. J. Charles, A. Kosmac, J. Krautschick, J.A. Simón, N. Suutala, and T. Taulavuori: *Austenitic Chromium–Manganese Stainless Steels—A European Approach*. Materials and Applications Series, 2012. https://www.worldstainless.org/media/lqrfojpy/austenitic_cr_mn_en.pdf. Accessed 28 Jan 2021.
4. E.I. Galindo-Nava and P.E.J. Rivera-Díaz-del-Castillo: *Acta Mater.*, 2017, vol. 128, pp. 120–34.
5. A.P. Marques de Oliveira, M. Houmard, W. da Silva Labiapari, and C. Godoy: *Metall. Mater. Trans. A*, 2019, vol. 50A, pp. 1663–71.
6. Y. Ikegami and R. Nemoto: *ISIJ Int.*, 1996, vol. 36, pp. 855–61.
7. A. Rezaee, A. Kermanpur, A. Najafzadeh, M. Moallemi, and H. Samaei Baghbadorani: *Materials*, 2013, vol. 46, pp. 49–53.
8. M. Moallemi, A. Kermanpur, A. Najafzadeh, A. Rezaee, H.S. Baghbadorani, and P.D. Nezhadfar: *Mater. Sci. Eng. A*, 2016, vol. 653, pp. 147–52.
9. A.S. Hamada, L.P. Karjalainen, R.D.K. Misra, and J. Talonen: *Mater. Sci. Eng. A*, 2013, vol. 559, pp. 336–44.
10. ASTM-International: *ASTM E8/E8M-13: Standard Test Methods for Tension Testing of Metallic Materials*, ASTM-International, West Conshohocken, 2013.
11. ASTM-International: *ASTM E21-09: Standard Test Methods for Elevated Temperature Tension Tests of Metallic Materials*, ASTM-International, West Conshohocken, 2017.
12. ASTM-International: *ASTM E139-11: Standard Test Method for Conducting Creep, Creep-Rupture and Stress-Rupture Tests of Metallic Materials*, ASTM-International, West Conshohocken, 2011.
13. ASTM-International: *ASTM E112-13: Standard Test Methods for Determining Average Grain Size*, ASTM-International, West Conshohocken, 2013.
14. A.S. Hamada, A.P. Kisko, P. Sahu, and L.P. Karjalainen: *Mater. Sci. Eng. A*, 2015, vol. 628, pp. 154–59.
15. AISI: *A Designers Handbook Series—No. 9004—High Temperature Characteristics of Stainless Steels*, AISI-American Iron and Steel Institute, 2020. https://nickelinstitute.org/media/1699/high_temperaturecharacteristicsofstainlesssteel_9004_.pdf. Accessed 28 Jan 2021.
16. J.J. Jonas, M.J. Luton: in *Advances in Deformation Processing*, J.J. Burke, et al., eds., Plenum Press, New York, 1978, pp. 215–42.
17. M. Li, Y. Duan, D. Yao, Y. Guan, and L. Yang: *Metals*, 2020, vol. 10, p. 64.

18. W.G. Kim, S.N. Yoon, and W.S. Ryu: *Key Eng. Mater.*, 2005, vol. 297, pp. 2272–77.
19. J.T. Boyle and J. Spence: *Stress Analysis for Creep*, Butterworth & Co. Ltd., 1988. ISBN 0408-01172-6.
20. K.R. Williams and B. Wilshire: *Met. Sci. J.*, 1973, vol. 7, pp. 176–79.
21. M.D. Mathew, G. Sasikala, K.B.S. Rao, and S.L. Mannan: *Mater. Sci. Eng. A*, 1991, vol. 148, pp. 253–60.
22. D.G. Morris and D.R. Harries: *Met. Sci. J.*, 1978, vol. 12, pp. 525–31.
23. M.E. Kassner and M.T.P. Prado: *Fundamentals of Creep in Metals and Alloys*, Elsevier Ltd., Amsterdam, 2004.
24. R. Viswanathan: *Damage Mechanisms and Life Assessment of High Temperature Components*, ASM International, Materials Park, 1989.
25. C. Zener and H. Hollomon: *J. Appl. Phys.*, 1944, vol. 15, pp. 22–27.
26. T.G. Langdon: *Strength of Metals and Alloys (ICSMA 6) Proceedings of the 6th International Conference*, Melbourne, Australia, R.C. Gifkins, ed., 1982, p. 1105.
27. S.A.A. Akbari Mousavi and M. Meisami: *Int. Conf. Metall. Mater.—METAL*, Roznov pod Radhostem, Czech Republic, 2010, pp. 1–10.
28. T. Zhuchkova, S. Aksenov, V. Shkatov, and I. Mazur: *J. Chem. Technol. Metall.*, 2018, vol. 53, pp. 354–59.
29. I. Rieiro, M. Carsí, and O.A. Ruano: *Mater. Sci. Technol.*, 2009, vol. 25, pp. 995–1002.
30. M. Erami, A.H. Daei-Sorkhabi, and F. Vakili-Tahami: *Int. J. Press. Vessel Pip.*, 2019, vol. 176, p. 103947.
31. E.C. Monkman and N.J. Grant: *An Empirical Relationship Between Rupture Life and Minimum Creep Rate in Creep-Rupture Tests—Proceeding of ASTM*, ASTM-International, West Conshohocken, 1956.
32. F. Garofalo: *ASTM/STP*, 1960, vol. 283, pp. 82–89.
33. V.L. Sordi and L.O. Bueno: *Mater. Sci. Eng. A*, 2008, vols. 483–84, pp. 498–501.
34. F. Dobes and K. Milicka: *Met. Sci.*, 1976, vol. 10, pp. 382–84.
35. G. Sundararajan: *Mater. Sci. Eng. A*, 1989, vol. 112, pp. 205–14.
36. E.I. Samuel, B.K. Choudhary, D.P.R. Palaparti, and M.D. Mathew: *Procedia Eng.*, 2013, vol. 55, pp. 64–69.
37. C. Phaniraj, B.K. Choudhary, K. Bhanu Sankara Rao, and B. Raj: *Scripta Mater.*, 2003, vol. 48, pp. 1313–18.
38. V. Sklenička, K. Kucharová, P. Král, M. Kvapilová, and J. Dvorak: *Kov. Mater.*, 2017, vol. 55, pp. 69–80.
39. M.F. Ashby and B.F. Dyson: *Advances in Fracture Research*, Pergamon Press, Oxford, 1984.
40. L.O. Bueno and V.L. Sordi: *Mater. Sci. Eng. A*, 2008, vols. 483–484, pp. 560–63.
41. L.O. Bueno and J.F.R. Sobrinho: *Matéria (Rio J.)*, 2012, vol. 17, pp. 1098–1108.
42. R.E. Schramm and R.P. Reed: *Metall. Trans. A*, 1975, vol. 6, p. 1345.
43. G.E. Dieter and D.J. Bacon: *Mechanical Metallurgy*, McGraw-Hill, New York, 1988.
44. M.D. Mathew, K. Laha, and V. Ganesan: *Mater. Sci. Eng. A*, 2012, vol. 535, pp. 76–83.
45. A.F. Smitll and R. Hales: *Met. Sci. J.*, 1975, vol. 9, pp. 181–84.

Publisher's Note Springer Nature remains neutral with regard to jurisdictional claims in published maps and institutional affiliations.